Smart Mater. Struct. 3 (1994) 18–25. Printed in the UK

Active enhancement of the absorbent properties of a porous material

Denis Thenail, Marie-Annick Galland and Michel Sunyach
Laboratoire de Mécanique des Fluides et d'Acoustique, URA CNRS 263,
Ecole Centrale de Lyon, 36 Avenue Guy de Collongue, 69131 Ecully Cedex, France

Received 8 June 1993, accepted for publication 27 August 1993

Abstract. We present in this paper an active anechoidal termination composed of a porous material, whose absorbent properties are improved by a secondary source. A simple model of acoustic propagation in a porous medium leads to optimal absorption criteria, which are verified by absorption coefficient measurements under normal incidence at the end of a Kundt duct. A secondary source is placed at the backward interface of the material, and imposes zero pressure by destructive interferences, which is a necessary condition for the maximum absorption. Several control set-ups are tested and provide the anechoism for broadband excitations.

1. Introduction

At present, the noise radiated by open-ended ducts can be reduced in two principal ways. Firstly, we can act during the acoustic propagation in the duct, by placing absorbent material along the wall linings. This passive method is generally used in vehicle mufflers and in air-conditioning silencers. Absorbents, made from porous materials, such as fiberglass, are very efficient at high frequencies. Unfortunately, the performance of the absorbents decreases rapidly with the frequency, even when a considerable thickness of material is used.

Secondly, we can also act at the end of the duct by minimizing the pressure in this section with an active control system [1, 2]. A set of secondary sources uses an upstream detection signal in order to create a pressure field, thus providing destructive interferences at several points. The efficiency of this technique requires a perfect correlation between the detection and control signals. Therefore, the case of a periodic noise generated by an internal combustion engine is particularly successful. The reference signal is synchronized with the rotation and an adaptive numerical filter follows the motor rating variations. Unfortunately, in several applications, the noise spectrum also contains an important broadband component, requiring a microphone as upstream detection in the duct [3]. In this case, we cannot assume the necessary coherence between signals because of a possible change of the acoustic wave during its propagation in the flow.

The inadequacy of these two passive and active methods leads to an alternative, consisting of the development of active wall linings able to absorb acoustic energy with an array of local control set-ups. Several teams have achieved, as a first task, an active anechoidal termination, consisting of a controlled source placed at the end of a standing wave duct. In the experiment presented by Guicking and Karcher [4], the control was achieved via an analog filter and a two-microphone probe, so as to detect and cancel the regressive wave, for a sinusoidal excitation in the 100–800 Hz frequency range. This technique was extended to the case of a broadband excitation with an adaptive numerical filter by Orduna-Bustamante and Nelson [5]. We conducted a similar experiment, but the impedance adaptation was controlled by the direct measurements of velocity and pressure close to the active termination, the velocity value being obtained via an accelerometer placed on the flat membrane of the secondary loudspeaker [6]. This technique could, in the future, allow an active control under oblique incidence, along the lateral boundaries of a duct.

Another design for active wall linings consists in improving the properties of a passive absorbent with active control. The work reported here, as in Guicking's experiments for pure tone excitations [7], presents the enhancement of the performances of a fiberglass sample, with active control, for a broadband of low frequencies.

Firstly, we examine the behavior of a porous material in a simple model, and deduce the optimal absorption conditions. Experimental investigations with a standing wave duct confirm the theoretical results. One of the main criteria is to place the absorbent at a quarter of wavelength from a hard surface, being equivalent to a zero pressure at the backward interface of the material sheet. This can be achieved by an active control and is necessarily required for a broadband excitation. Several controllers are used, each of them providing very good absorption over a large frequency range.

0964-1726/94/010018 + 08 $19.50

2. Modeling of the propagation in a porous medium

An absorbent porous material such as fiberglass, is composed of filaments and cells, immersed in the surrounding fluid. The absorption efficiency of such a material results from the balance of two competing effects: the penetration depth of sound waves into the medium, which increases with cell size, and the dissipation of incident sound energy by friction, which decreases with cell size. In order to model wave penetration and dissipation in such a material, we represent the porous medium as a bundle of tubes of radius a, aligned with the direction of propagation of the incident wave. The porosity of the material is therefore completely defined by the radius of the tubes (figure 1).

We make two assumptions to simplify the analysis. First, the friction in the tube is modeled by a global force, which acts opposite to the acoustic velocity. Second, the exchange of heat between the fluid and the solid is very intense and the process is considered isothermal. The linearized equations can then be written as follows:

state equation of gas:

$$p = \frac{P_0}{\rho_0}\rho \tag{2.1}$$

equation of mass conservation:

$$\frac{\partial \rho}{\partial t} + \rho_0 \frac{\partial u}{\partial x} = 0 \tag{2.2}$$

equation of momentum conservation:

$$\rho_0 \frac{\partial u}{\partial t} = -\frac{\partial p}{\partial x} - Ru \tag{2.3}$$

where R is a positive constant, related to the viscosity, μ, of the ambient fluid and to the porosity, a, of the material. For a steady laminar flow in a cylindrical duct, R equals $16\mu/a^2$. In our case the flow is non-stationary and the instantaneous pressure gradient cannot be balanced by the friction. Therefore, we arbitrarily put:

$$R = \frac{8\mu}{a^2}. \tag{2.4}$$

This is done to relate the friction in the tubes to the viscosity and the porosity in a realistic manner. By eliminating the density and velocity fluctuations in the system of equations, we obtain:

$$\frac{\partial^2 p}{\partial x^2} - \frac{\rho_0}{P_0}\frac{\partial^2 p}{\partial t^2} - \frac{R}{P_0}\frac{\partial p}{\partial t} = 0. \tag{2.5}$$

The solution is represented in the form of a monochromatic damped wave:

$$p(x, t) = A\,\mathrm{e}^{\mathrm{i}(\omega t - kx)}$$

where k is a complex wavenumber. The characteristic equation is given by:

$$-k^2 + \frac{\rho_0}{p_0}\omega^2 - \frac{R}{p_0}\mathrm{i}\omega = 0. \tag{2.6}$$

Let us introduce the isentropic sound speed c_0 and the incident wavenumber $k_0 = \omega/c_0$, then

$$k^2 = \gamma k_0^2\left(1 - \frac{R\mathrm{i}}{\rho_0 c_0 k_0}\right) \tag{2.7}$$

where γ is the ratio of specific heats of air. We deduce the wavenumber for the progressive wave:

$$k = k_0\sqrt{\frac{\gamma}{2}}(\sqrt{X+1} - \mathrm{i}\sqrt{X-1}) \tag{2.8}$$

where:

$$X = \sqrt{1 + \left(\frac{R}{\rho_0 c_0 k_0}\right)^2}. \tag{2.9}$$

The expression of acoustic velocity is obtained from the mass conservation equation:

$$\frac{\partial u}{\partial x} = -\frac{1}{\rho_0}\frac{\partial \rho}{\partial t} = -\frac{\mathrm{i}\omega}{P_0}p \tag{2.10}$$

which gives, for the progressive wave:

$$u = \frac{\gamma k_0}{\rho_0 c_0 k}p. \tag{2.11}$$

In order to verify this model, we study the reflection of a wave incident to the boundary at a semi-infinite porous medium (figure 2).

The index 1 characterizes the ambient fluid and the index 2, the porous medium. The coordinate x is measured from the interface. Progressive and regressive

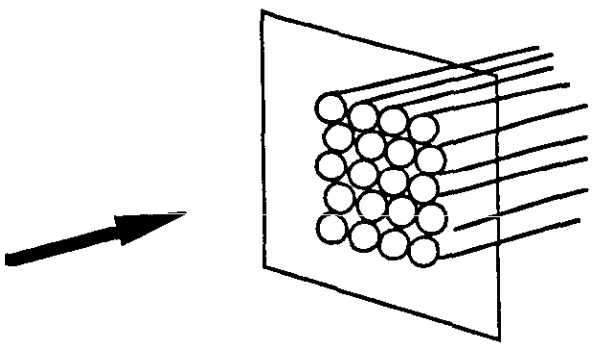

Figure 1. Schematic diagram of a porous material.

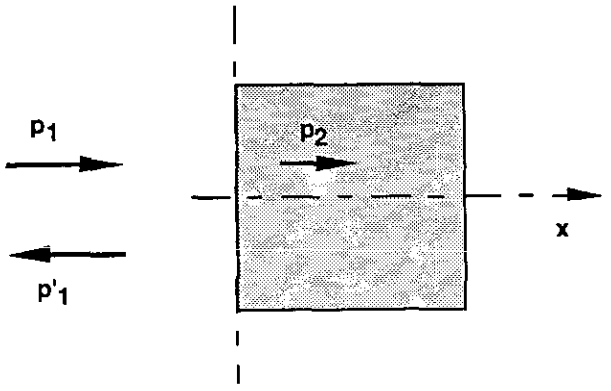

Figure 2. Reflection on a semi-infinite porous medium.

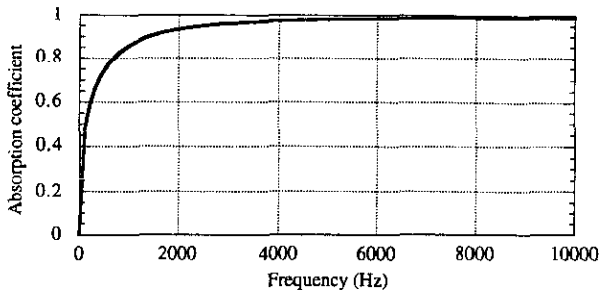

Figure 3. Theoretical absorption curves in the case of a semi-infinite porous medium.

pressure waves are given by:

$$\begin{cases} p_1 = A_1 e^{-ik_0 x} \\ p_1' = B_1 e^{ik_0 x} \\ p_2 = A_2 e^{-ikx} \end{cases} . \tag{2.12}$$

At the interface, the continuity of pressure and velocity leads to:

$$\begin{cases} A_1 + B_1 = A_2 \\ A_1 - B_1 = \gamma \dfrac{k_0}{k} A_2 \end{cases} . \tag{2.13}$$

We then deduce the absorption coefficient at normal incidence:

$$\alpha_n = 1 - \left|\frac{B_1}{A_1}\right|^2 = 1 - \left|\frac{k - \gamma k_0}{k + \gamma k_0}\right|^2 . \tag{2.14}$$

The behavior of α_n is reported in figure 3. At low frequencies, the absorption is small, while at high frequencies, α_n tends to a limit: $4\sqrt{\gamma}/(1+\sqrt{\gamma})^2$ near to 1 (0.993 for air). So we can conclude that this model leads to a behavior in harmony with the experimental results.

3. Absorbent of finite thickness

3.1. Expression of the absorption coefficient

Here, we will state the conditions that maximize the absorption of a finite-thickness porous material. As reported in figure 4, a porous material of thickness d is placed at a distance e from a rigid boundary. We use the same notation as in the previous section. The absorbed and reflected waves can be written for each medium as follows:

$$\begin{cases} p_1 = A_1 e^{-ik_0 x} \\ p_1' = B_1 e^{ik_0 x} \end{cases} \quad \begin{cases} p_2 = A_2 e^{-ikx} \\ p_2' = B_2 e^{ikx} \end{cases} \quad \begin{cases} p_3 = A_3 e^{-ik_0 x} \\ p_3' = B_3 e^{ik_0 x} \end{cases} . \tag{3.1}$$

The boundary conditions for this problem are given by:

continuity of pressure and velocity at $x = 0$

$$\begin{cases} A_1 + B_1 = A_2 + B_2 \\ A_1 - B_1 = \gamma \dfrac{k_0}{k}(A_2 - B_2) \end{cases} \tag{3.2}$$

continuity of pressure and velocity at $x = d$

$$\begin{cases} A_2 e^{-ikd} + B_2 e^{ikd} = A_3 e^{-ik_0 d} + B_3 e^{ik_0 d} \\ \gamma \dfrac{k_0}{k}(A_2 e^{-ikd} - B_2 e^{ikd}) = A_3 e^{-ik_0 d} - B_3 e^{ik_0 d} \end{cases} \tag{3.3}$$

total reflection on the support, at $x = d + e$

$$A_3 e^{-ik_0(d+e)} - B_3 e^{ik_0(d+e)} = 0 \tag{3.4}$$

This leads to the reflection coefficient:

$$r = \frac{B_1}{A_1} = \frac{\begin{array}{l} e^{ikd}(1+\beta+\alpha(1-\beta))(\alpha-1) \\ +e^{-ikd}(1+\beta-\alpha(1-\beta))(\alpha+1) \end{array}}{\begin{array}{l} e^{ikd}(1+\beta+\alpha(1-\beta))(\alpha+1) \\ +e^{-ikd}(1+\beta-\alpha(1-\beta))(\alpha-1) \end{array}} \tag{3.5}$$

with:

$$\alpha = \frac{k}{\gamma k_0}$$

$$\beta = e^{-2ik_0 e} .$$

The absorption coefficient at normal incidence is then deduced by $\alpha_n = 1 - |r|^2$.

The variation of α_n with the frequency for a fixed porosity and thickness is shown in figure 5. The different curves correspond to distinct values of e. Note that the

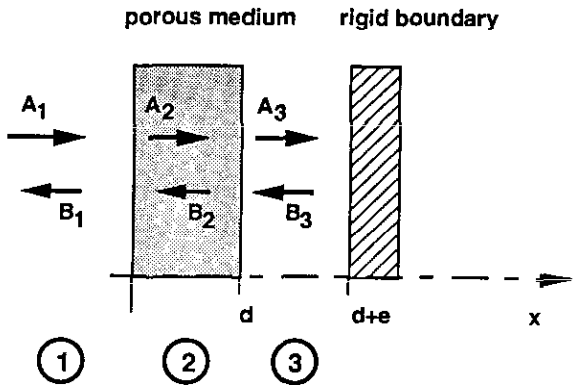

Figure 4. Reflection on a finite-thickness porous medium.

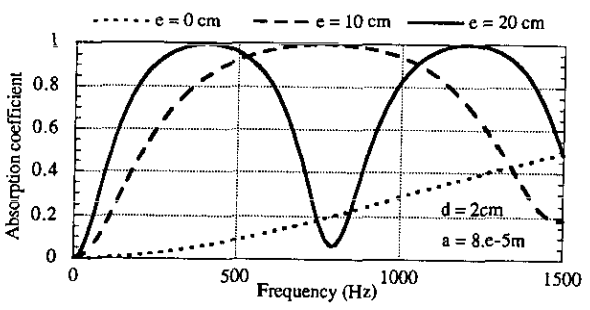

Figure 5. Theoretical absorption curves in the case of a finite-thickness porous material.

absorption is maximum when the space e corresponds to one quarter of the wavelength, or to one of its odd multiples: $e = (2n+1)(\lambda/4)$, which is equivalent to $k_0 e = (2n+1)(\pi/2)$. Therefore, the material is particularly weakly absorbent when it is directly adjacent to the rigid support. On the other hand, for the maximum absorption frequencies, and considering the total reflection on the rigid boundary, we deduce that:

$$p(d) = A_3 \, e^{-ik_0 d}(1 + e^{-2ik_0 e}) = 0.$$

Consequently, at these frequencies, the velocity is maximum at the interface $x = d$, and the attenuation of energy in the material, due to viscous effects, will also be maximum.

3.2. Characterization of the optimal absorption

In the case presented above, the maximum absorption coefficient is near to 1. However, this value may be much smaller under certain conditions. When maximum absorption occurs, we have $e = \lambda/4$, and formula (3.5) becomes, putting $\beta = -1$:

$$r = \frac{e^{ikd}(\alpha - 1) - e^{-ikd}(\alpha + 1)}{e^{ikd}(\alpha + 1) - e^{-ikd}(\alpha - 1)} \qquad (3.6)$$

We now proceed to show how the thickness or porosity of the material and the excitation frequency influence the absorption.

The variation of the maximum absorption coefficient with the material thickness, at different frequencies, is shown in figures 6 and 7. Figure 6 shows a low frequency range, and figure 7 a higher. The value of porosity equals 8×10^{-5} m, which corresponds approximately to the fiberglass used in the experiments described below. For low frequencies, we note that there is an optimal thickness for which the absorption coefficient is near to 1 at every frequency. This thickness is small (2 cm in the case of fiberglass), which is somewhat contrary to intuition. As the thickness increases, the curves approach a constant value, which is frequency dependent. This constant level corresponds to the absorption due to a semi-infinite porous medium and increases with the frequency, as previously seen in paragraph 1.

The behavior for the high-frequency case is very different. There is no longer an optimal thickness, but

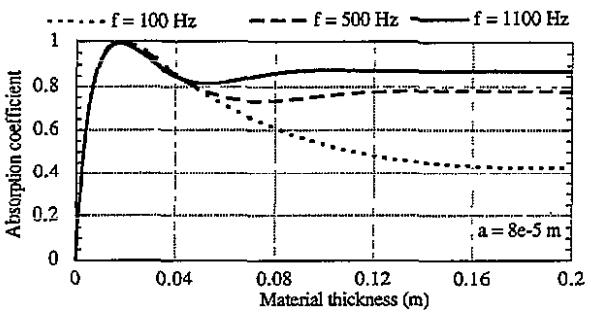

Figure 6. Variations of the maximum absorption coefficient with the material thickness for a fixed porosity and three low frequencies.

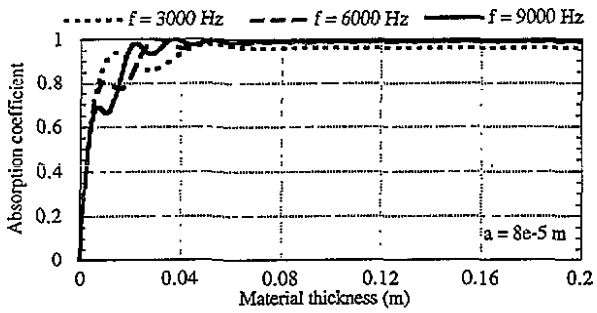

Figure 7. Variations of the maximum absorption coefficient with the material thickness for a fixed porosity and three high frequencies.

for large thickness, the absorption is almost perfect at all frequencies.

The dual nature of the frequency response suggests the existence of a critical frequency, which we will try to determine from the basic equations.

At low frequencies, the equation of momentum conservation leads to the predominance of viscous over inertial forces. Let R_a be the ratio between viscous and inertial effects:

$$R_a = \frac{\rho_0 \omega}{R} \qquad (3.7)$$

and let us introduce f_{crit}, the critical frequency corresponding to $R_a = 1$. Thus,

$$f_{crit} = \frac{R}{2\pi\rho_0} = \frac{4\mu}{\pi\rho_0 a^2}. \qquad (3.8)$$

For $f < f_{crit}$, the following approximations are then justified:

$$k^2 = \gamma k_0^2 \left(1 - \frac{\bar{R}i}{\rho_0 c_0 k_0}\right) \approx -\frac{\gamma k_0 \bar{R}i}{\rho_0 c_0} \qquad (3.9)$$

and for a small thickness of material

$$r = \frac{i\tan(kd)\alpha - 1}{i\tan(kd)\alpha + 1} \approx \frac{ikd\alpha - 1}{ikd\alpha + 1} \qquad (3.10)$$

therefore

$$r = \frac{ik^2 d - \gamma k_0}{ik^2 d + \gamma k_0}. \qquad (3.11)$$

Replacing k^2 by expression (3.9), we obtain

$$r = \frac{Rd - \rho_0 c_0}{Rd + \rho_0 c_0} \qquad (3.12)$$

which is frequency independent. For the thickness given by:

$$d_{opt} = \frac{\rho_0 c_0}{R} = \frac{\rho_0 c_0 a^2}{8\mu} \qquad (3.13)$$

the reflection coefficient r equals 0 and the absorption is total at every frequency.

In the example presented above, the direct application of this last formula leads to an optimal thickness of 2 cm, with a critical frequency of approximately 2500 Hz.

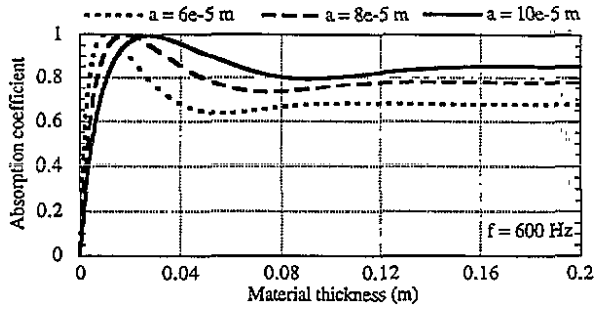

Figure 8. Variations of the maximum absorption coefficient with the material thickness for three porosities and a fixed low frequency.

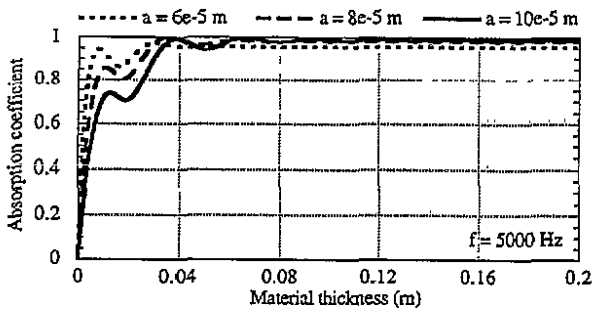

Figure 9. Variations of the maximum absorption coefficient with the material thickness for three porosities and a fixed high frequency.

In conclusion, a maximum absorption at low frequencies can be obtained, contrary to what might be expected, with a small thickness of material, as long as the material properties and distance from the rigid wall are correctly chosen.

On the other hand, for frequencies higher than the critical frequency, inertial effects due to the penetration into the material predominate. In this case, the absorption increases with the amount of material, approaching the behavior of a semi-infinite medium.

The maximum absorption coefficient has a similar variation with porosity, for a fixed frequency. At low frequencies (600 Hz in figure 8), we see that the optimal thickness increases as the porosity increases, in accordance with equation (3.13). The tubes of the material become wider and the friction weaker. At higher frequencies (5000 Hz in figure 9), the absorption level reached for a large thickness absorbent increases with the porosity, the wider tubes improving the penetration of the acoustic wave.

3.3. Active control of the absorbent

According to the preceding section, the following criteria must be used to increase the efficiency of the absorbent.

(i) First, for $f > f_{crit}$, a sufficient thickness of material must be employed. The absorption graphs tend to show the value required to be at minimum

$$2d_{opt} \approx \frac{2\rho_0 c_0}{R} = \frac{\rho_0 c_0 a^2}{4\mu}.$$

(ii) On the other hand, two conditions for low-frequency excitation must also be observed: the material thickness must be equal to d_{opt} and the material must be positioned at one quarter of a wavelength from the rigid boundary.

For broadband excitation, one cannot meet this criterion. However, as shown in section 3.1, this is equivalent to zero pressure at the interface $x = d$, a result for which active control is well designed, as we now explain. A secondary source replaces the rigid wall. This source is then controlled to obtain, by superposition, the zero pressure desired for maximum absorption in the whole frequency range of excitation.

4. Experimental results

In order to verify our model, we carried out an experimental program. The initial aim was to compare the measurements with the predictions for the passive absorption, and then to show the feasibility of using active control to increase the absorption.

4.1. Experimental set-up

A rigid duct, with a square cross section ($12 \times 12\,cm^2$) is used for the experiments, as shown in figure 10. One end is closed with a loudspeaker and the other with the porous material, an ordinary fiberglass sample. The backward cavity is closed to a rigid movable boundary, which enables the distance e to be variable. The source generates waves whose frequency never exceeds the 1400 Hz duct plane wave cut-off. This allows us to use the method of Chung and Blaser [8] to determine the absorption coefficient. It is based on the measure of transfer functions between two fixed microphones, separated by a distance of 3 cm. Then the frequency range allowed for measurement goes from 200 Hz to 1400 Hz.

4.2. Characterization of porous material

We first tested a fixed thickness of material, while changing the distance e. A comparison between the absorption graphs so obtained and the model is shown in figure 11. The fitting has been found with a porosity of 8×10^{-5} m. We observe that the curves have basically the same shape. More precisely, the maximum absorption is obtained for $e = (2n+1)(\lambda/4)$, corresponding to an absorption coefficient α_n, which is close to 1. Note that the experimental minima are

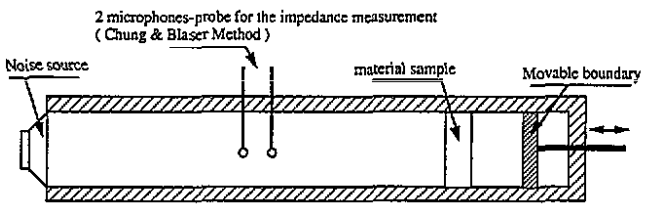

Figure 10. Experimental set-up.

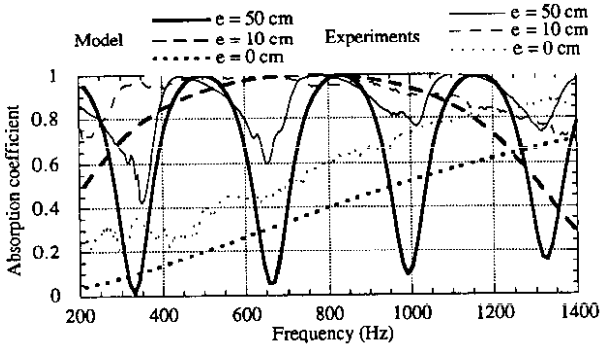

Figure 11. Theoretical and experimental absorption curves for a finite-thickness porous material.

distinctly higher than the theoretical values, probably caused by the imperfectly rigid boundary behind the fiberglass.

Next we varied the thickness of the fiberglass, in order to find the optimal amount of material, which is a low frequency characteristic. Figure 12 shows the variation of absorption coefficient versus frequency for four different thicknesses, from 1 to 4 cm. The maximum value of 1 is obtained for a thickness of 2 cm. A smaller absorption is observed with a lesser or a greater thickness of fiberglass, supporting the value calculated in the model (figure 5). For large thickness (figure 13), the maximum absorption defined by the theoretical semi-infinite medium is reached and both curves follow the same path.

These experiments demonstrate the general validity of our model, even allowing for the underestimation of the absorption obtained in practice.

4.3. Active optimization of the absorbent

In the experimental configuration, the rigid end of the cavity is now replaced by a loudspeaker (figure 14). The controller pilots this secondary source, so as to minimize the pressure at the interface $x = d$, where the control microphone is located.

Theoretically, the value of the distance e is no longer important. Nevertheless, the experiments show that the results are better when e is very small, owing to the easier achievement of the zero pressure condition. In addition this set-up is very compact, which is a great advantage.

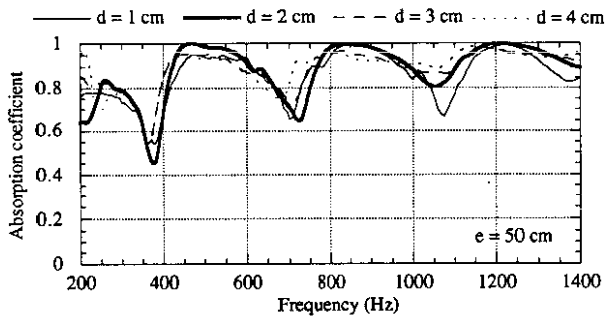

Figure 12. Experimental absorption curves for four material thicknesses.

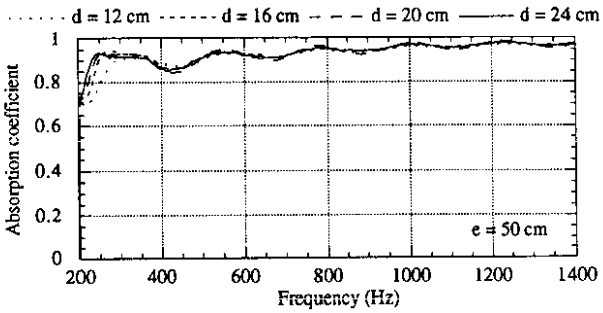

Figure 13. Experimental absorption curves for four larger thicknesses.

Different detection signals and controllers are used in order to study the two following points.

(i) First of all we will verify that the zero pressure at $x = d$ leads effectively to an increased absorption. To do this, we make use of the most suitable configuration: a detection at the primary source and an adaptive numerical filter.

(ii) We are also interested in showing the feasibility of this set-up in realistic situations, where local detection is definitely required.

4.3.1. Detection at the primary source. In order to evaluate the limit behavior of this active control, detection is first taken at the primary source. We also use a numerical filter, which is designed and developed at the Laboratoire de Mécanique des Fluides et d'Acoustique. The hardware signal processing includes an Analog Devices ADSP 2101 digital signal microprocessor. The adaptive updating of the filter coefficients is processed by the 'filtered-X' least mean square (LMS) algorithm. The experiment is performed with a filter length set to 150 coefficients, and the sampling frequency to 8 kHz.

The global cancellation at the control microphone is 20 dB. Thus the absorption coefficient measured in the frequency range 200–1400 Hz is approximately 1 (figure 15). We should point out that, even without active control, the elasticity of the secondary loudspeaker results in an improvement of the absorbent behavior, as compared with the rigid-wall case.

We also attempt to verify the model conclusions concerning optimal thickness. For pure tone excitations, the obtained cancellation at the sensor is 40 dB. Seven

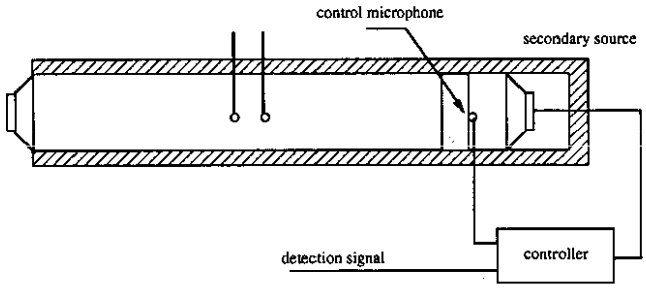

Figure 14. Standing wave duct with the active termination.

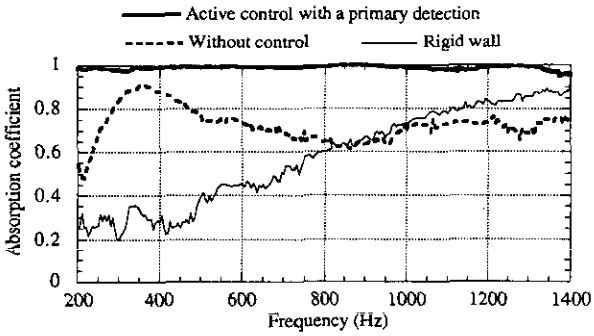

Figure 15. Experimental absorption curves when the secondary source provides a broadband zero pressure at the material backward interface with an adaptive filter and a primary detector.

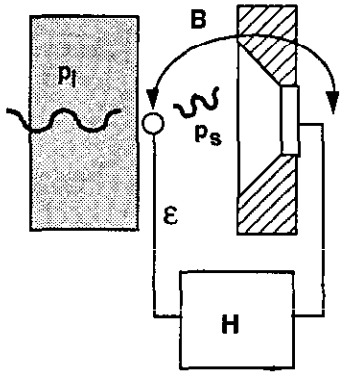

Figure 17. Active absorbent using anti-noise helmets control design.

frequencies, from 200 to 800 Hz, are tested, each of them with several thicknesses, from 1 to 20 cm (figure 16). These lead to the same findings as the model prediction: the maximum absorption corresponds to an optimal thickness of approximately 2 cm. When $d > d_{opt}$, we also note that the absorption increases with the frequency.

4.3.2. Configuration with a local detection. In practice, the primary signal is never at one's disposal. In addition, a total coherence of the acoustic wave during its propagation between the detection and the control points is required, a situation rarely obtained. In this case, a local detection becomes necessary.

B: Electroacoustic transfer function.

The classical zero-pressure technique developed in the anti-noise helmets by Carme [9] is first employed (figure 17).

The purpose here is to minimize the ratio:

$$\frac{p_i + p_s}{p_i} = \frac{1}{1 - HB} \tag{4.1}$$

which represents the obtained attenuation. This closed-loop configuration cannot be controlled by a numerical filter; we employ the standard 'bi-quad' analog filter with 2 poles and 2 zeros. Figure 18 shows that the absorption decreases as frequency increases. As usual with such a set-up, the poor loudspeaker response limits the performance. A closed-loop instability occurs at 1800 Hz, when $HB = 1$.

Next, we placed a microphone upstream of the fiberglass sample, at the interface $x = 0$, as shown in figure 19.

In this figure, A and B are the transfer functions between the secondary source and the control and detection microphone, respectively, and H_0 is the transfer function between the detection and control microphones, due to the primary source alone.

The optimal transfer function of the filter is then given by:

$$H_{opt} = \frac{-H_0}{B - AH_0}. \tag{4.2}$$

Considering the behavior of the measured optimal phase, the criterion of control is, for frequencies above 500 Hz, to maintain a mean phase shift of 35 degrees. The 'bi-quad' filter provides roughly this function and hence, the absorption coefficient is equal to 1 in the range 500–1400 Hz (figure 20).

5. Conclusions

The simple model of propagation in a porous medium presented here is largely supported by experimental results. In order to optimize the performances of an absorbent material, the following features are required.

(i) For frequencies greater than f_{crit}, a thickness of

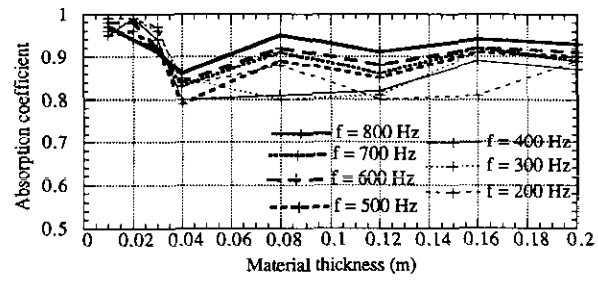

Figure 16. Experimental variations of the maximum absorption coefficient with the material thickness.

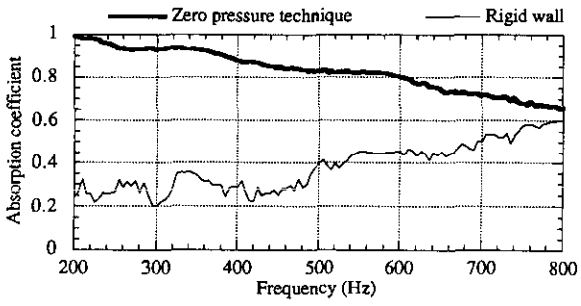

Figure 18. Absorption curves when the active termination set-up includes the anti-noise helmet control design.

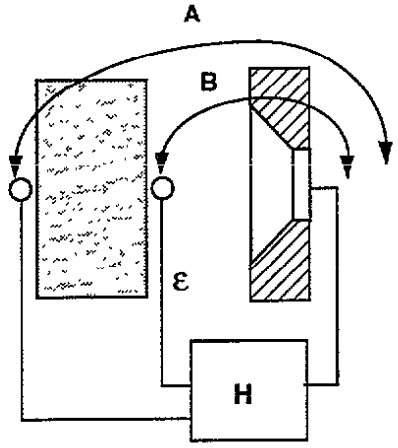

Figure 19. Active absorbent with a detector at the front of the material interface.

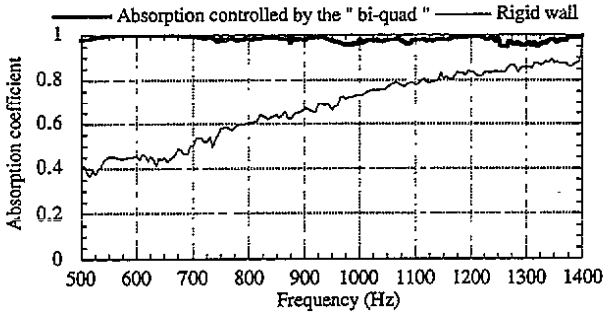

Figure 20. Absorption curves with an upstream local detector and an analog filter.

material greater than $\rho_0 c_0 a^2/4\mu$ provides excellent absorption.

(ii) The absorption of low frequencies requires a precise optimal thickness of $d_{opt} = \rho_0 c_0 a^2/8\mu$ and the use of an active control able to impose zero pressure at the backward interface. A simple analog filter, which satisfies the local detection condition for a broadband excitation, serves this purpose very well.

Further development must include the behavior of the active absorbent when the incidence is oblique, or even grazing. This work will form the basis for the design of active absorbent panels.

References

[1] Ross C F 1982 Application of digital filtering to active control of sound *Acustica* **51** 135–40

[2] Roure A 1985 Self adaptive broadband active sound control system, *J. Sound Vib.* **101** 429–41

[3] Billoud G 1988 Développement d'un filtre numérique adaptatif contrôlant les phénomènes de bouclage—Application à l'absorption acoustique active *Thèse de Doctorat* Université Lyon I, no 88–182

[4] Guicking D and Karcher K 1984 Active impedance control for one-dimensional sound *ASME J. Vib. Acoustics, Stress Reliab. Des.* **106** 393–6

[5] Orduna-Bustamante F and Nelson P A 1992 An adaptive controller for the active absorption of sound *J.A.S.A.* **91** 2740–7

[6] Thenail D and Galland M A 1992 Development of an active anechoidal boundary *Paper W4 Workshop Contrôle Actif, Idée Force 92 Eur'Acoustique, Lyon*

[7] Guicking D and Lorenz E 1984 An active sound absorber with porous plate *ASME J. Vib. Acoust. Stress Reliab. Des.* **106** 389–404

[8] Chung J Y and Blaser D A 1980 Transfer function method of measuring in-duct acoustic properties *J.A.S.A.* **68** 907–22

[9] Carme C 1988 Absorption acoustique active dans les cavités auditives *Acustica* **66** 233–46